IJST, Transactions of Mechanical Engineering, Vol. 37, No. M2, pp 133-147
Printed in The Islamic Republic of Iran, 2013

CANARD-WING INTERACTIONS IN SUBSONIC FLOW*

S. SAMIMI[1],** A. R. DAVARI[2] AND M. R. SOLTANI[3]

[1, 2]Dept. of Mech. and Aerospace Eng., Science and Research Branch, Islamic Azad University, Tehran, I. R. of Iran
Email: salva_samimi@yahoo.com
[3]Dept. of Aerospace Eng., Sharif University of Technology, Tehran, I. R. of Iran

Abstract– Extensive subsonic wind tunnel tests were conducted on a coplanar wing-canard configuration at various angles of attack. In these experiments, a 60° swept canard was placed upstream of a 60° swept main delta wing. This paper deals with the distribution of mean and fluctuating pressure coefficients on the upper surfaces of both the canard and the wing immersed in a variety of angles of attack. According to the results, presence of canard postpones the vortex formation and growth on the wing to higher angles of attack compared to the canard-off case. Due to the canard downwash field, the wing operates at lower effective angles of attack and therefore, its vortex breakdown is delayed. The spectral analysis of the unsteady pressure on both the canard and the wing show the existence of narrow, dominant frequency band containing the majority of the fluctuation energy. This frequency band is believed to be the natural frequency of the leading edge vortex. The results show that the dominant frequency of the wing vortex is lower than that of the canard having the same sweep angle as the wing, which is an indication of the wing vortex attenuation due to canard downwash field.

Keywords– Canard, delta wing, pressure power spectrum, leading edge vortex

1. INTRODUCTION

The use of canards in advanced aircraft for control enhancement and for improved aerodynamic performance is a topic of continued interest and research. In addition to providing maneuver control and trim, the influence of canards on wing aerodynamics often increases maximum lift and decreases trim drag. In many canard-configured aircraft, the main benefits of canards are realized during maneuver or other dynamic conditions.

For close-coupled canards, the aerodynamic performance associated with the canard-wing interaction is of particular interest. The presence of a canard in close proximity to the wing results in a highly coupled canard-wing flowfield interactions which includes downwash/upwash effects, vortex-vortex interactions and vortex-surface interactions. The use of canards for improved performance has been supported by numerous experimental investigations as well as some recent computational studies.

An early experimental study by Behrbohm [1] indicated the potential use of closed-coupled canard configurations for improved aerodynamic characteristics based on the canard-wing interaction. It has been found that the value of maximum lift coefficient and the corresponding angle of attack can be increased considerably by adding a delta canard to a delta wing.

Gloss and McKinney [2], and Gloss [3, 4] provided insight into the effects of canard geometry and position on the aerodynamic loading of a typical canard-wing-body combination. An extensive experimental study was conducted by Hummel and Oelker [5, 6], which concentrated on the canard and

*Received by the editors April 11, 2012; Accepted October 15, 2013.
**Corresponding author

wing vortex systems. They provided details into the mechanisms of the vortices interaction. They also traced vortex trajectories and determined the effect of the canard vortices on the surface pressure distribution over the wing.

The experimental study by Howard and Kersh [7] provided detailed information on the flow structure of deflected canard geometries in the low subsonic regime and has shown encouraging results towards the optimization of such configurations.

Up to 1990, the experimental surveys were generally concentrated on the canard-wing configurations without taking the fuselage effects into account. In 1993, Howard [8] tested a canard- wing model including fuselage. A tertiary vortex was observed at the juncture of canard and fuselage that had an impact on the resulting flowfield and was not evident in the studies of wing-canard combinations in the absence of body.

Zhiyong [9] studied the effect of position and platform of canard-wing configurations on the burst process of the leading edge vortices of a double delta wing as well as the aerodynamic characteristics of a fighter configuration equipped with a double delta wing. Based on these findings, he proposed an optimum fighter configuration with canard and a double delta wing

Hayashibara et al. [10] during an experimental study in a water tunnel investigated the effect of a canard-on delta wing vortices of a high canard-wing configuration. They exploited the die flow visualization technique to observe the vortex breakdown location and its variations during dynamic pitch-up and pitch-down motions with varying pitch rates. They found that compared to canard-off configuration, there is a delay in vortex breakdown due to the presence of the canard and the dynamic pitch motion. The most favorable delay was obtained when the canard was located very closed to the main delta wing and the model was pitched up at a fast rate or pitched down at a slow rate.

Guy et al. [11, 12] conducted an experimental investigation to study the effects of canard shape on the aerodynamic characteristics and performance of a generic canard-wing-body configuration. They examined the effects of canard aspect ratio, sweep angle and taper ratio on the aerodynamic loads of the configuration in subsonic flow. They proposed a new method to evaluate the canard efficiency by measuring moment-to-drag ratio

Bergmann and Hummel [13] examined the body-wing-canard configurations in a symmetrical flow. Their results indicate that the effects of canard vortex on the flow over the wing are considerable for large deflections and for a low canard position, i.e. the canard surface is much lower than that of the wing. However, at very low canard positions, this favorable interference effect vanishes. The vortex breakdown on the canard deteriorates the vortical flow at all angles of attack and leads to a considerable loss of lift.

Close-coupled canard configurations have also been the subject of computational studies for a long time. Numerical computations of flow fields around such configurations show encouraging agreement with the available experimental data. Tu [14, 15] studied transonic flow over a canard–wing–body configuration by means of thin-layer Navier–Stokes equations. He calculated the strong effect of the canard vortex on the strength, reattachment, and separation of the wing vortex. He further calculated the effect of the canard-on the surface pressure distribution. Similar solutions were performed by Ekaterinaris [16] for the configuration studied by Hummel et al. [5, 6] at low subsonic speeds. He limited his analysis to laminar flow computations for 20 degrees incidence only, but confirmed the delay of vortex breakdown resulting from the canard and obtained good agreement with Hummel's data.

Tuncer and Platzer [17] investigated the subsonic flow field over a close-coupled delta canard-wing-body configuration at high angles of attack using a Navier-Stokes solver. They presented their results in terms of particle traces, surface streamlines and leeward-side surface pressure distributions for both

canard-on and canard-off configurations. They found that the presence of the canard delays the wing vortex breakdown to positions aft of the wing trailing edge.

Recently, the optimization algorithms were employed to optimize the canard shape and position by either numerical or analytical methods. These optimizations were, for instance, to reduce the sonic boom reduction and improve the lift to drag ratio for supersonic transports [18] or to achieve a desired trim flight control force [19], etc.

Nearly all studies undertaken so far were concentrated on the canard effects on the forces and moments of the aircraft or the canard signature on the flow field over the wing. Though valuable information has already been obtained on the effects of canard-on the flow field over the wing, to the authors' knowledge, the upstream influence of wing on the canard as well as the power spectrum analysis of canard and wing vortices have seldom been studied.

In the present research, effects of canard-on the wing flow field and wing on the canard were investigated in a canard-wing-body configuration. The results include the surface pressure distribution on wing and canard as well as the wing alone pressure data as a benchmark to study the canard-wing flow interactions. The frequency content of instantaneous pressure fluctuations on both the wing and the canard were estimated using the power spectral density (PSD) function of the unsteady component of the differential pressure coefficient. The differential pressure time histories from each test condition were converted into the frequency domain using Discrete Fourier Transform (DFT) techniques. The average PSD functions were obtained by averaging the Discreet Fourier transforms. The dominant frequencies of the instantaneous pressure were identified from the power spectral density plots. The results can be thought of as a different view point to the vortex interaction phenomenon. These findings can be extensively used in all canard-wing vehicles at moderate to high angles of attack in a subsonic flow.

2. MODEL AND EXPERIMENTAL APPARATUS

The present experiments have been carried out in a closed circuit, 80×80 cm subsonic wind tunnel. The maximum attainable speed in the test section is 100 m/sec and the Reynolds number varies between 5.29×10^5 and 5.26×10^6 per meter. Turbulence intensity in the test section has been measured to be less than 0.1%.

This investigation has been performed on a coplanar close-coupled canard-wing-body configuration. Figure 1 shows the model installed in the test section. Both the wing and the canard have delta planforms of aspect ratio 1.17 and 1.15 respectively, and a corresponding leading-edge sweep of 60°. They were made of aluminum alloy and attached to a half-body fuselage.

64 and 27 pressure tabs were carefully drilled on the upper surface of the wing and the canard respectively. Fig. 2 shows the pressure tabs position on both the wing and the canard. Each tab was connected to a sensitive pressure transducer to measure the surface pressure distribution on both planforms.

The experiments were conducted at a nearly constant air speed of 60 m/sec corresponding to a Reynolds number of 1.11×10^6 based on the wing root chord. The model angle of attack was varied from 10° to 30°. All data were acquired by an AT-MIO-64E-3 data acquisition board capable of scanning 64 channels at a rate of 500 KHz.

Total errors encountered in the pressure measurements including the accuracy of the electronic devices such as transducers and acquisition board as well as the errors imparted to the data due to flow angularity and blockage effects were estimated by analytical approaches [20, 21]. Both the single sample precision and the bias uncertainty in the pressure measurement were also taken into account. Based on the method mentioned in the above references, the overall uncertainty for the presented data is less than ± 3.0%.

Figure 3 shows the result of a typical data uncertainty analysis on wing and canard surface pressure measurements.

3. RESULTS AND DISCUSSION

The experiments consisted of real time pressure measurements on both canard and wing in the canard-wing configuration. A canard-off configuration was also examined as well for comparison. Since both the wing and the canard have the same sweep angles, the differences in the corresponding flowfields are believed to be due to up and down stream influences of these lifting surfaces on each other as well as the fuselage flowfield. A power spectrum analysis was also conducted on the surface pressure values, determining the vortex behavior on wing and canard.

Figure 4 shows the results of surface pressure distribution at different angles of attack for both the canard-on and canard-off configurations at several chordwise stations. The leading-edge vortex signature can be detected from the suction peaks on both configurations. An interesting point observed in Fig. 4 is the location of the vortex core on the wing. For wing in presence of canard, i.e. canard-on case, the wing vortex is shifted towards the leading edge, while for the canard-off case the core was closer to the wing root. At small to moderate angles of attack, the absolute value of pressure on the wing for canard-off configuration is slightly lower than that for the corresponding canard-on case for x/c's near the wing trailing edge.

In other words, for the canard-on configuration, the suction peaks on the wing surface pressure at front regions are higher than those for the canard-off cases, while at the rear near the wing trailing edge, the value of the suction peak for the canard-on configuration has been reduced. So it can be inferred that the domain of favorable influence of the canard is mostly restricted to the front and middle parts of the wing at moderate to high angles of attack.

From Fig. 4, for the canard-off configuration at 20 degree angle of attack, the vortex breakdown seems to occur at the rear part of the wing, Fig. 4a. This is in accordance with the existing experimental data for a simple 60 degree swept wing [22]. At $\alpha=30°$, the vortex structure over the wing surface in canard-off case has nearly been destroyed for all sections shown in Fig. 4, while for the canard-on configuration the wing vortex is still active throughout the wing and the suction peak can be observed in the pressure distribution at this angle of attack. On the other hand, canard induces behind its trailing edge a downwash field within its span and an upwash field outside its span. The downwash field reduces the effective angle of attack in the inner portion of the wing considerably, and this leads to a suppression of flow separation there. The upwash field increases the effective angle of attack in the outer portions of the wing, and this supports flow separation there.

This mechanism postpones formation and breakdown of the wing vortex for canard-on configuration. Because of the nonuniform distribution of the effective angle of attack along the leading edge of the wing, the wing vortex is fed with vorticity in a different manner than is known from the canard-off configurations. Generally speaking, the wing in presence of canard, works at a lower effective angle of attack than an isolated wing.

The canard surface pressure distributions are shown at four longitudinal positions in Fig. 5 for various angles of attack. The pressure distribution on the canard is very similar to that of the wing for the canard-off configuration shown in Fig. 4, except for the trailing-edge region, where the absolute values of surface pressure on the canard seem to be increased compared to the corresponding locations on the wing alone. This is especially the case for high angles of attack, where the burst flow is dominated on the rear part of the wing with substantially lower pressures than those at moderate angles of attack. However, on the rear part of canard at high angles of attack, the amount of suction is obviously higher than that of the

wing having the same sweep angle. This is believed to be due to the favorable acceleration effect from the wing up to 25 degrees angle of attack, which is due to wing upwash effect, Figs. 5c and d.

The spectral content of the differential pressure fluctuations at an angle of attack of 15 degrees at four chordwise positions is illustrated in Fig. 6. For all positions examined here, the energy content of the flow field is mainly concentrated in a relatively narrow frequency band in the range of 7 to 10 Hz with the dominant frequency of about 8.5 Hz. This frequency is believed to be associated with the wing leading edge vortex. The accumulated energy in this limited band may be an indication of a periodic or quasi periodic fluctuation which is due to the swirling vortex pattern.

This peak in the pressure power spectrum occurs at about the same frequency over the entire surface of the wing while its amplitude is clearly different for each position. The power spectrum at x/c = 0.313 shows a smaller peak compared to the two next chordwise locations. It seems that the vortex structure at this location on the wing surface has been deteriorated by the canard flow and therefore, the small peak in the power spectrum at x/c = 0.313 is the canard vortex signature on the wing, Fig. 6a. At x/c=0.563 and 0.688 the peak value at the dominant frequency shows a remarkable increase, Figs. 6b and 6c.

Strong peaks and high oscillations are expected from the points on the wing located either on the way of the wing leading edge vortex or the extension of the canard vortical flow. At x/c=0.563, maximum value of the power spectrum occurs at point 21, which means that at this angle of attack and chordwise position, the vortex core is very close to this point.

At x/c=0.875, Fig. 6d, the dominant frequency is the same as that for the other chordwise locations, while the peak value at this frequency, which is an indication of the vortex energy level, is clearly lower than that measured at other positions. The leading edge vortex near the trailing edge at this angle of attack lifts off from the surface and the pressure tabs located on the wing surface receive less influence from it.

Further, at low to moderate angles of attack, the domain of the favorable influence of canard is mostly restricted to the front and middle portions of the wing. This has been shown to attenuate the wing vortex strength near the trailing edge [22].

In addition to the dominant peak corresponding to the wing vortex natural frequency, another characteristic frequency, lower than the former, with smaller amplitude is observed in the power spectrum. The large eddy formation in the wake region of canard may be the reason for this low frequency excitation. A few high frequency random fluctuations are also observed, which are probably caused by the strong interaction of the wing and the canard vortices. These high frequency excitations in the power spectrum can also be due to the energetic vortices shed from the nose and body, which have been shown to improve the flowfield over the wing at moderate to high angles of attack [22]. It should be noted that some of the random fluctuations are also caused by the tunnel noise as well as the free stream turbulence. However, according to hot wire measurements, the turbulence level in this tunnel was less than 0.1%.

For further insight, the power spectra for some neighboring points at two middle chordwise sections x/c=0.563 and x/c=0.688 on the wing at different angles of attack are shown in Fig. 7. Evidently, the amplitude of the dominant frequency changes with angle of attack due to changes in vortex strength and position. As noted earlier, for point 21 the maximum amplitude occurs at $\alpha=15°$ and decreases with increasing the angle of attack, Fig. 7a. Spectral content of pressure fluctuations at point 22, Fig. 7b, shows that for both angles of attack of 20 and 25 degrees the amplitudes of the dominant frequency peaks are significantly larger than those for point 21 at the same angles of attack. This suggests that the position of vortex core moves from point 21 to 22, i.e. toward the body, as increasing the angle of attack.

The same argument seems to be true for points 30 and 31 at x/c=0.688, Fig. 7c and 7d. For all angles of attack examined here, the amplitudes of the dominant frequency mode for point 31 are larger than those of point 30 and therefore the vortex core can be deduced to be closer to point 31 near the body. Apart from the vortex movement towards the body as increasing angle of attack, the vortex lift-off from the body may

also be responsible for decreasing the dominant frequency peak with angle of attack. Furthermore, for all points at 20 and 25 degrees angle of attack, the dominant frequency decreases. This gradual decrease of the characteristic frequency is likely a consequence of canard and wing vortex merging which occurs at moderate to high angles of attack.

A dramatic change occurs in the spectral density at $\alpha=30°$ and the dominant frequency increases to about 9.5 Hz due to the wing leading edge vortex breakdown. This value may correspond to the frequency of the burst vortex. The dominant peak at this angle of attack results from the strong interaction of the unsteady structure of vortex breakdown with the wing surface. As the vortex breakdown occurs, the region of high pressure scatters and propagates over the wing and imposes a certain degree of random fluctuations to the surface pressure field. In particular, the low-frequency region in the pressure power spectrum begins to rise rapidly due to vortex breakdown at all points on the wing.

The pressure power spectra on the canard surface are shown in Fig. 8 for two chordwise locations at 15 degrees angle of attack. As can be seen, the power spectra for the canard are similar to those for the wing. However, compared to the wing results, the amplitude of the dominant frequency mode is considerably smaller, especially at x/c=0.615, Fig. 8a, compared to x/c=0.563, Fig. 6b, on the wing. Further, the dominant frequency on the canard pressure power spectrum, for all cases, is larger than that for the wing.

Since the sweep angles for both the wing and the canard are the same, i.e. 60°, the differences between the pressure spectra of these two surfaces are associated with the canard wake and the vortex effects on the wing. Comparing Fig. 8a with Figs. 6b and 6c at nearly the same chordwise positions, the increased number of the oscillatory modes in the wing pressure power spectrum due to presence of the canard is obvious. It also seems that the canard decreases the frequency of vortex formation over the wing. Comparing the power spectra at x/c=0.615, Fig. 8a and x/c=0.769, Fig. 8b, at the latter, an increase is observed in the power spectrum intensity to a value about twice as large as that at the former station while the dominant frequency is nearly constant for both.

To achieve better insight, the variation of power spectrum for neighboring points at mentioned chordwise positions on canard are presented in Fig. 9 at different angles of attack. The results illustrate that with increasing angle of attack, the spectrum intensity is amplified due to an increase in the strength of the leading edge vortex, and frequency bandwidth decreases. Furthermore, the vortex trajectory shifts inboard as increasing the angle of attack.

At $\alpha=20°$, pressure fluctuations begin to rise rapidly with multiple peaks. This is a clear indication of vortex burst phenomenon. The pressure fluctuations at this angle of attack result from the strong interaction of the unsteady structure of vortex breakdown with the canard surface. With further increase in angle of attack a characteristic increase in surface pressure fluctuations is observed due to vortex bursting, especially when the burst location moves toward the apex.

Figures 10 through 13 show the downstream influence of canard-on the wing as well as the upstream influence of wing on the canard at four chordwise sections. Since both the wing and the canard have the same sweep angles, the flow patterns on either of them can be compared to that of another. According to Fig. 10a at $\alpha=10°$, the wing pressure on the suction side, which is an indication of the vortex strength, for the wing alone is higher than either the wing or canard in the canard-wing configuration.

This implies that the presence of canard decreases the vortex strength on the wing and, on the other hand, the wing does the same on the canard. However, in canard-wing configuration the drop in vortex strength for wing downstream of canard is higher than that for canard upstream of wing.

According to Figs. 10c and 10d at high angles of attack, the canard-on configuration show a higher performance than the canard-off case. As before, the favorable effect of wing on the canard is stronger than that of canard-on the wing with equal sweep angles.

Thus, in canard-wing interaction at low angles of attack, the flowfield on the wing at the front sections is more deteriorated than the corresponding sections on the canard. At high angles of attack, the isolated wing at canard-off configuration is shown to have a lower performance than either of the wing and the canard in canard-on configuration. However, the upstream influence of the wing on the canard is still more favorable than the downstream influence of the canard-on the wing.

Similar behavior can be observed in Fig. 11 at x/c=0.563. At all angles of attack, the canard upstream of the wing experiences a stronger suction than the wing downstream of canard, both having the same sweep angles. Compared with the isolated wing, Fig. 11 shows that the canard performance due to presence of wing is higher than that of the wing in presence of canard. This clearly indicates the favorable effect of wing on the canard and the adverse impact of canard-on the wing at the front regions of both surfaces. Note that at this middle chordwise station, the wing alone (canard-off) configuration has a better performance than the wing in presence of canard for a wide range of angle of attack.

A noteworthy problem in Fig. 11 is the vortex position. The wing vortex downstream of the canard is shifted outboard towards the wing tip, while the canard vortex upstream of the wing is observed to be moved inboard towards the root compared to the wing alone configuration. This phenomenon is believed to be due to the wing upwash effect on the canard and that of canard downwash on the wing.

According to the experimental investigations for a 60 degree swept wing, the vortex burst point reaches the trailing edge at an angle of attack of about 16 degrees [23]. For higher angles of attack, i.e. 20, 25 and 30 degrees, shown in Figs. 11b, 11c and 11d, the burst point occurs on the wing and canard surfaces moving towards the leading edge as the angle of attack increases.

From Fig. 11d, it seems that the vortex burst position at $\alpha=30°$ has reached about x/c=0.563 for isolated wing. At this angle of attack, a vortex is seen on the wing in presence of canard which has not been observed on the wing alone. This vortex may be induced by the canard vortical flow, which formed a suction region on the wing and the burst vortex has been retrieved.

For the two rear sections x/c=0.688 and 0.875 shown in Figs. 12 and 13, the canard upstream of the wing still shows a better aerodynamic behavior than the wing alone configuration. In these two sections at moderate to high angles of attack, the maximum value for the suction on the wing in presence of canard is a little higher than that for wing alone with a more concentrated vortical flow region.

Further, in all of these figures, the canard vortex was pushed towards the root and the wing vortex has been displaced towards the tip in comparison to the vortex position for wing alone configuration. This phenomenon, as stated earlier, is due to the wing upwash effects on the canard as well as the canard downwash effects on the wing and is observed at both low and high angles of attack.

4. CONCLUSION

An in-depth study has been undertaken on a coplanar wing-canard configuration in subsonic flow to study the impact of canard-on the wing and that of the wing on the canard in a relatively wide angle of attack range. Both the wing and the canard in these experiments had equal sweep angles of 60 degrees. The results show that canard postpones the vortex formation, growth and burst on the wing to some higher angles of attack compared to the isolated wing configuration. This favorable effect of canard-on the wing is restricted to the front and middle portions of the wing at low to moderate angles of attack. On the other hand, the wing was observed to induce a favorable flowfield on the canard at all angles of attack, especially at the rear region of the canard. This implies that the upstream influence of wing on canard amplifies the canard vortex strength and pushes it towards the root, while the downstream influence of canard-on the wing displaces the wing vortex towards the tip and at low angles of attack, decreases its

strength at the front parts of the wing. However, at high angles of attack, the canard is shown to have a favorable impact on the wing at the front parts. The pressure power spectrum analysis on both the canard and the wing shows that the dominant frequency of the leading edge vortex on the wing in presence of canard is smaller than that on the canard having the same sweep angle in presence of wing. It can be inferred that the downstream influence of canard, apart from its different effect on the wing at front and rear regions, has decreased the wing vortex energy level, showing the diffusive character of the downwash effects along with the dissipative effects of canard wake on the wing for both small and large angles of attack.

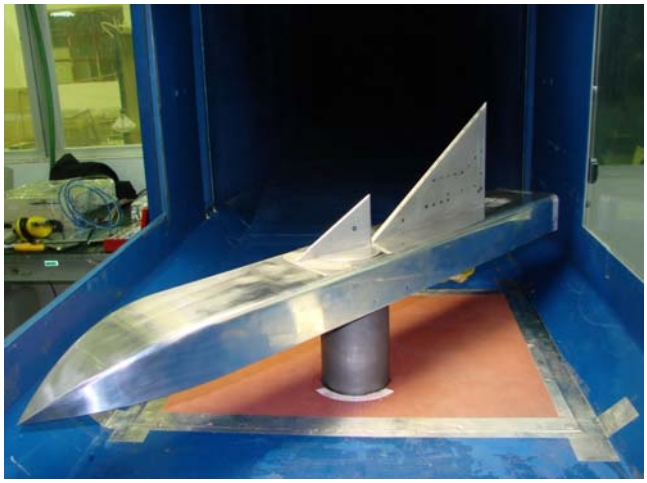

Fig. 1. The model installed in the test section

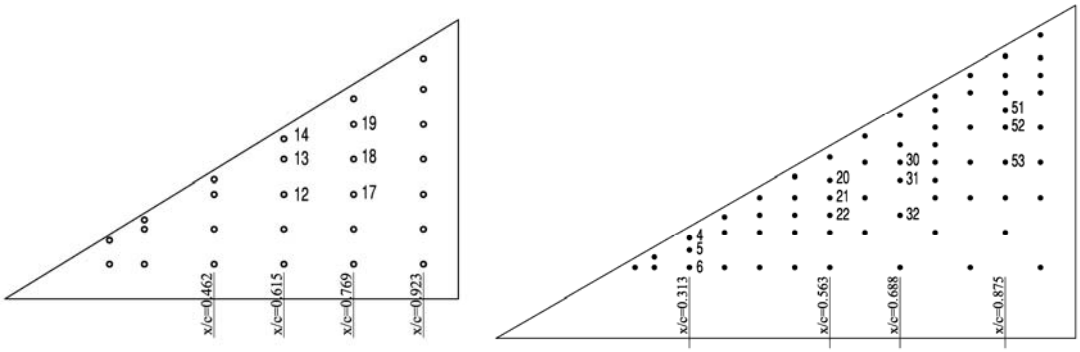

(a) Canard (b) Wing

Fig. 2. The positions of the pressure tabs

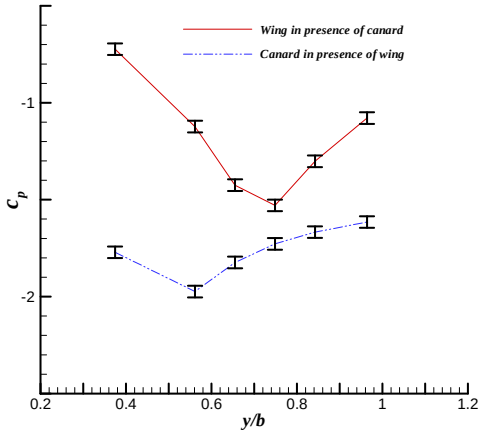

Fig. 3. Typical data uncertainty analysis

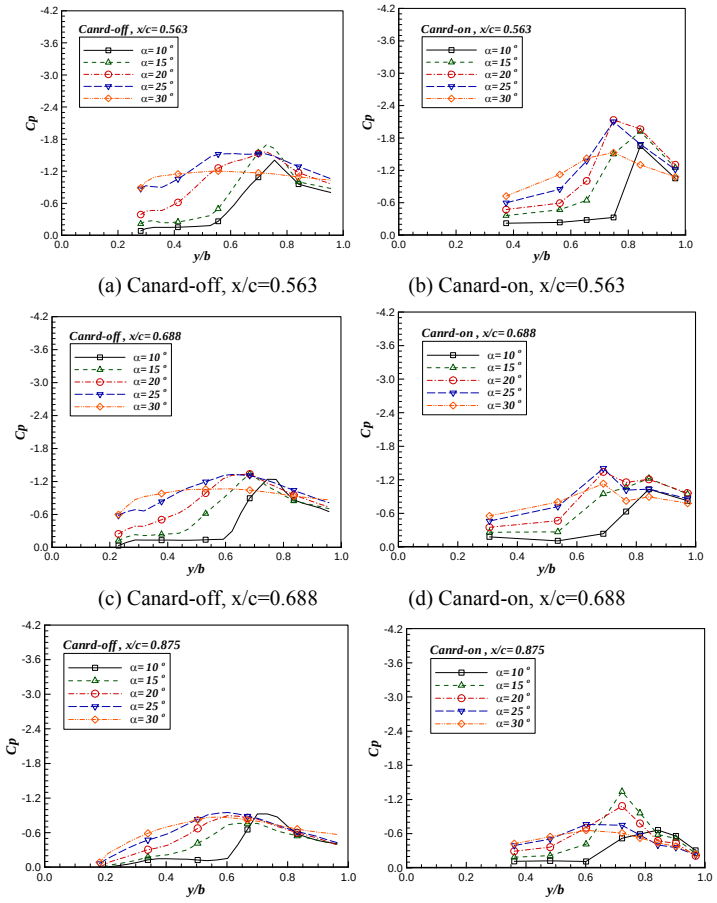

(a) Canard-off, x/c=0.563 (b) Canard-on, x/c=0.563

(c) Canard-off, x/c=0.688 (d) Canard-on, x/c=0.688

(e) Canard-off, x/c=0.875 (f) Canard-on, x/c=0.875

Fig. 4. Canard effects on spanwise pressure distribution on the wing

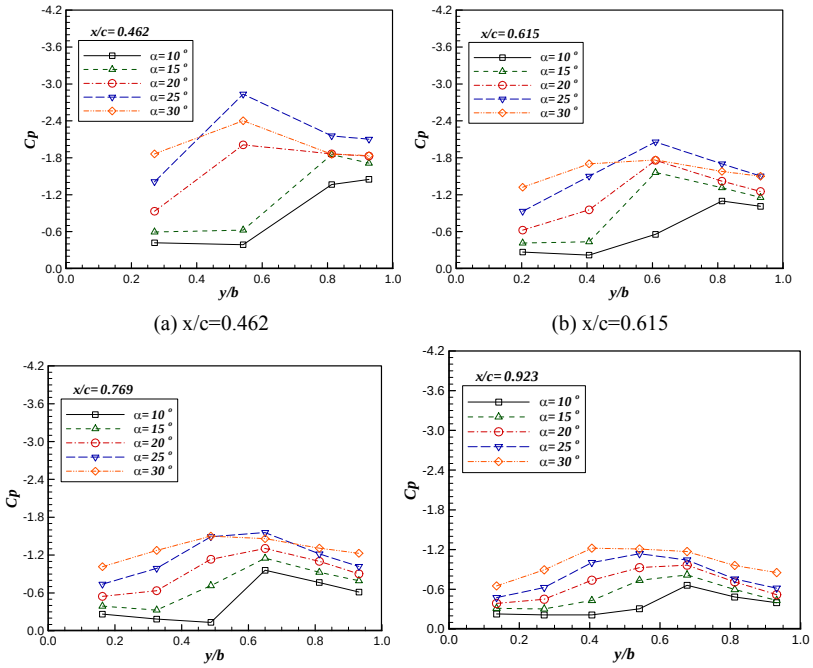

(a) x/c=0.462 (b) x/c=0.615

(c) x/c=0.769 (d) x/c=0.923

Fig. 5. Canard surface pressure distribution

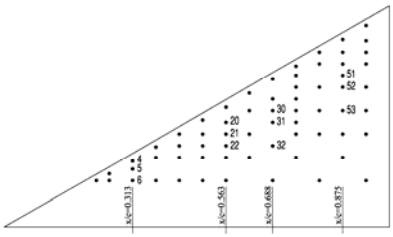

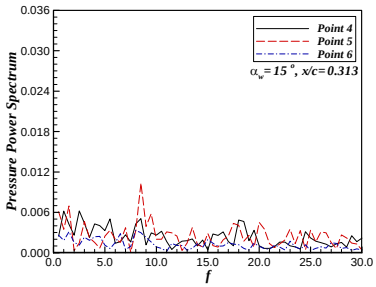

(a) x/c=0.313

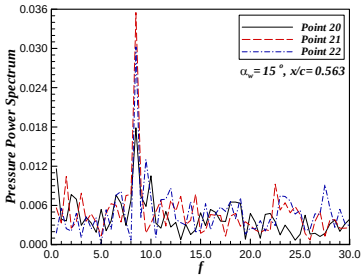

(b) x/c=0.563

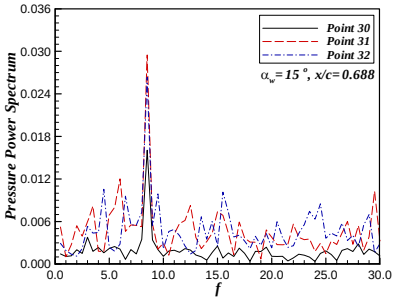

(c) x/c=0.688

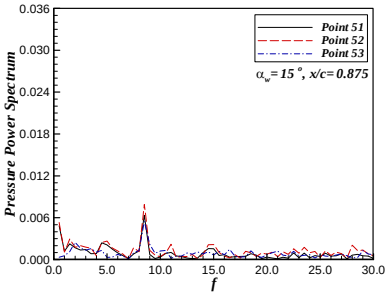

(d) x/c=0.875

Fig. 6. Wing pressure power spectrum, α=15°

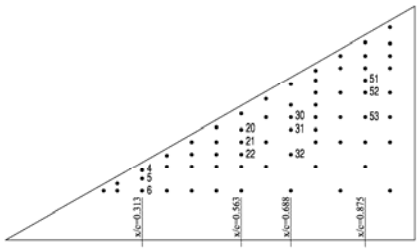

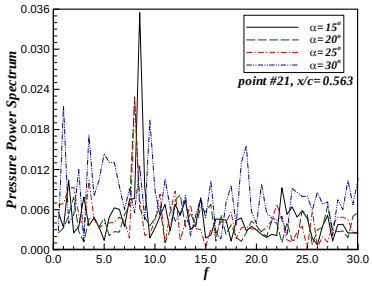

(a) x/c=0.563, point #21

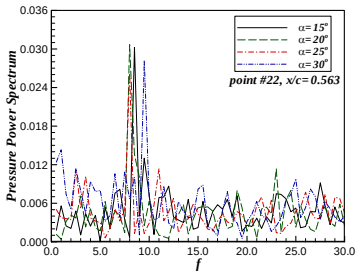

(b) x/c=0.563, point #22

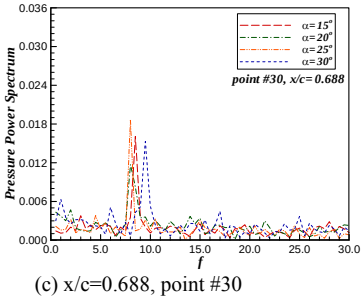

(c) x/c=0.688, point #30

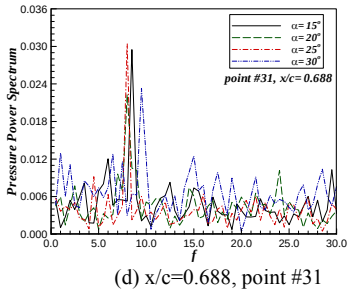

(d) x/c=0.688, point #31

Fig. 7. Wing Pressure power spectrum for neighboring points

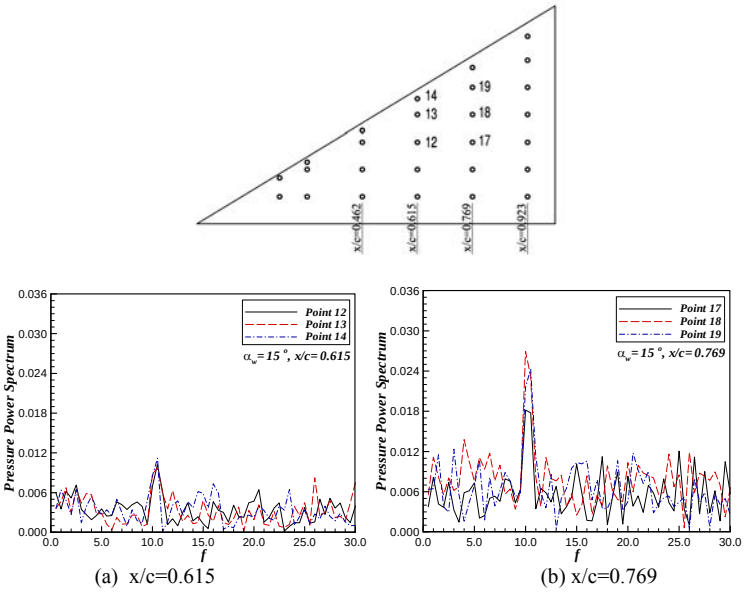

(a) x/c=0.615 (b) x/c=0.769

Fig. 8. Canard pressure power spectrum, α=15°

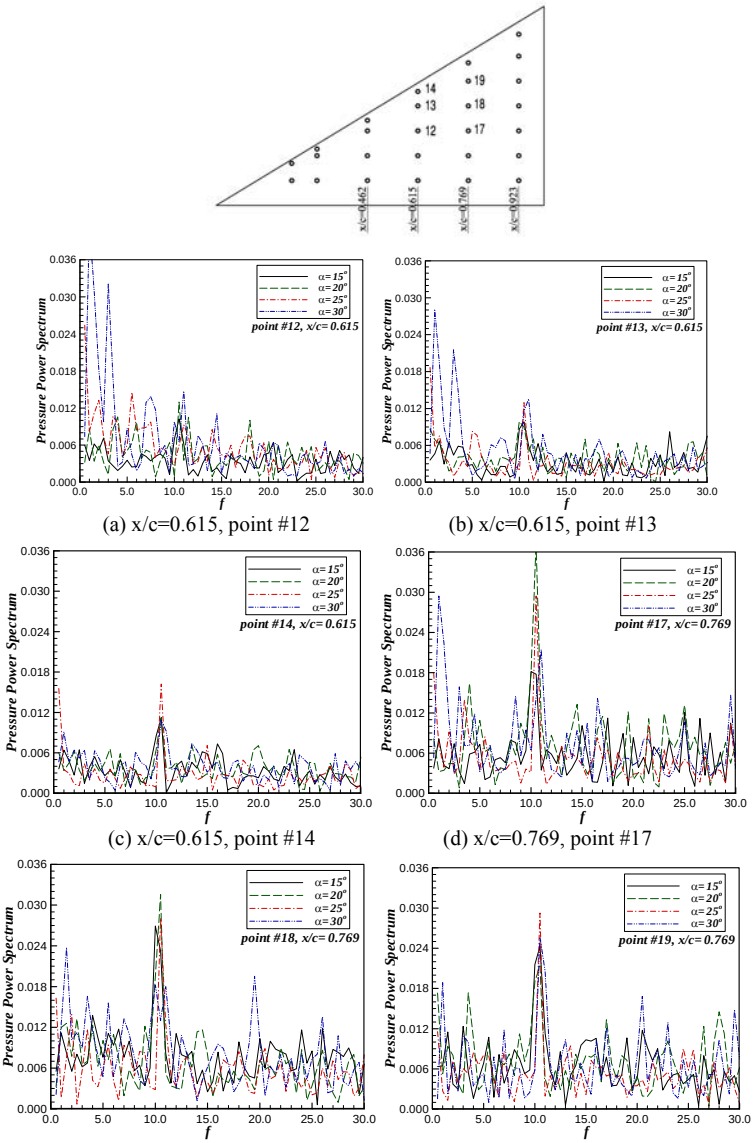

(a) x/c=0.615, point #12 (b) x/c=0.615, point #13

(c) x/c=0.615, point #14 (d) x/c=0.769, point #17

(e) x/c=0.769, point #18 (f) x/c=0.769, point #19

Fig. 9. Canard pressure power spectrum for neighboring points

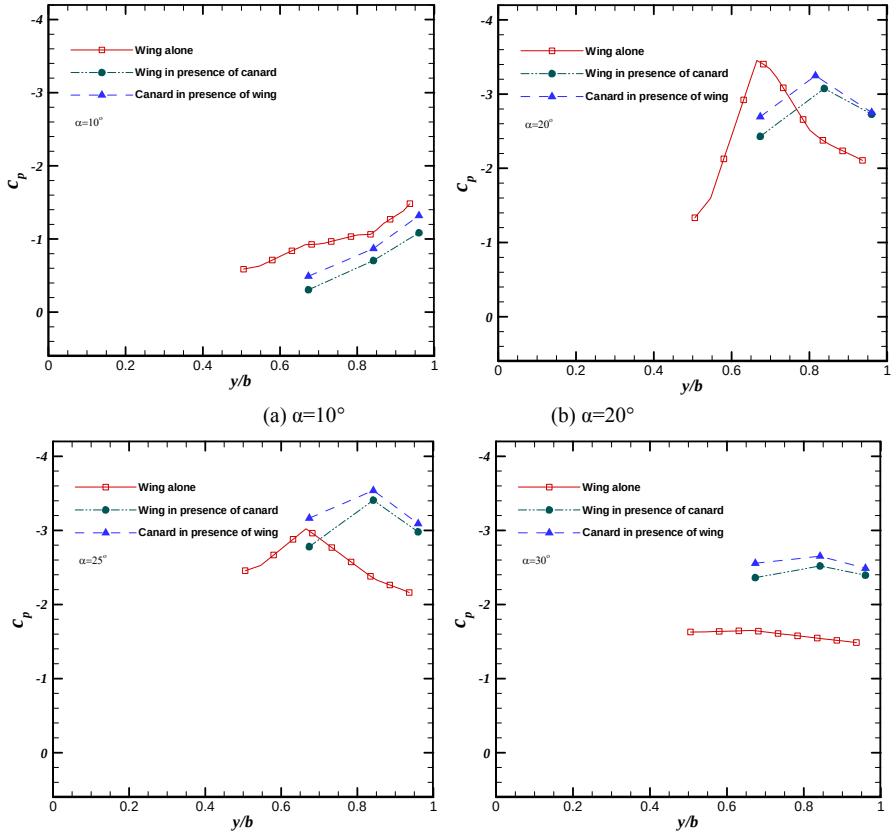

(a) α=10° (b) α=20°

(c) α=25° (d) α=30°

Fig. 10. Spanwise pressure distribution at x/c=0.313

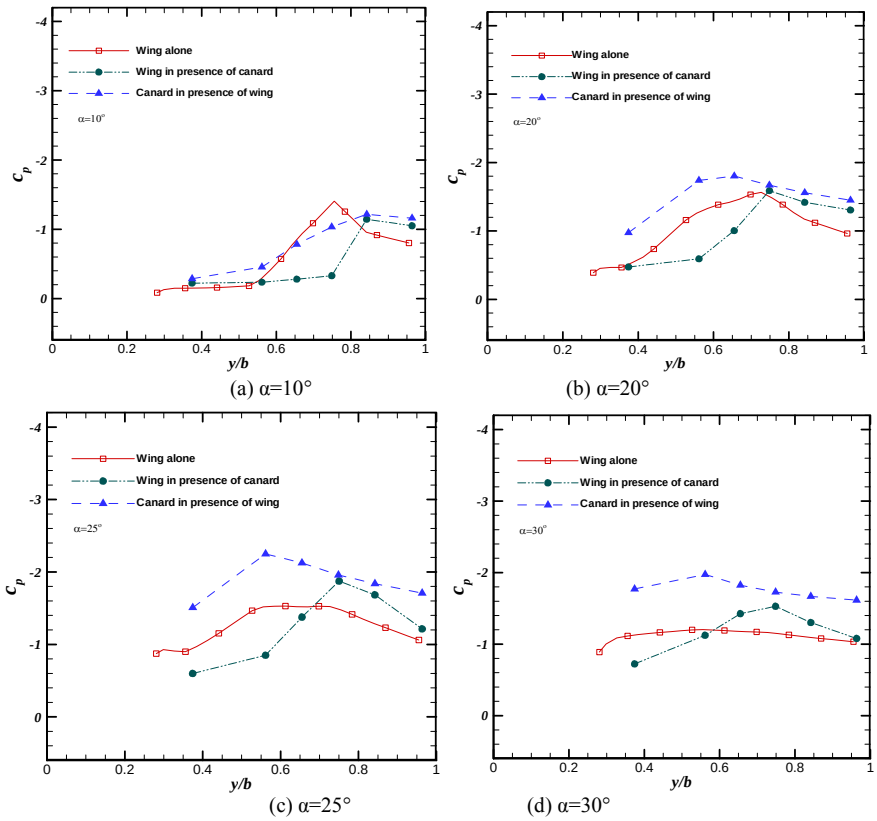

(a) α=10° (b) α=20°

(c) α=25° (d) α=30°

Fig. 11. Spanwise pressure distribution at x/c=0.563

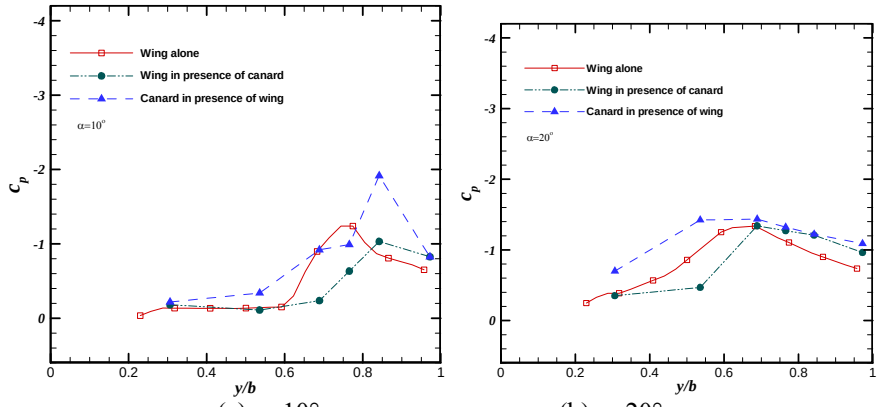

(a) α=10° (b) α=20°

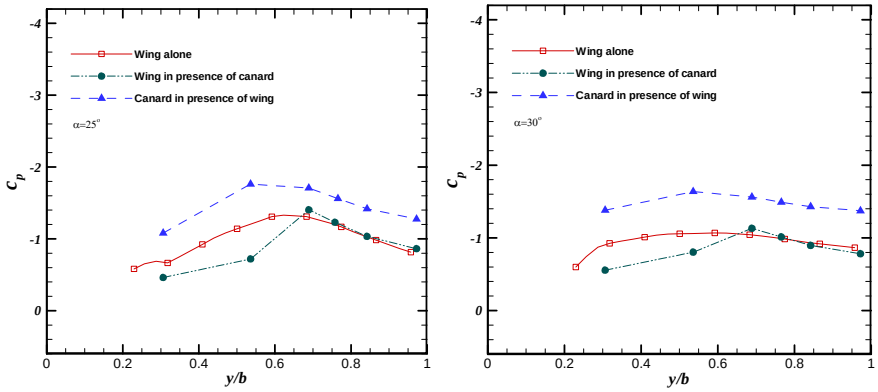

(c) α=25° (d) α=30°

Fig. 12. Spanwise pressure distribution at x/c=0.688

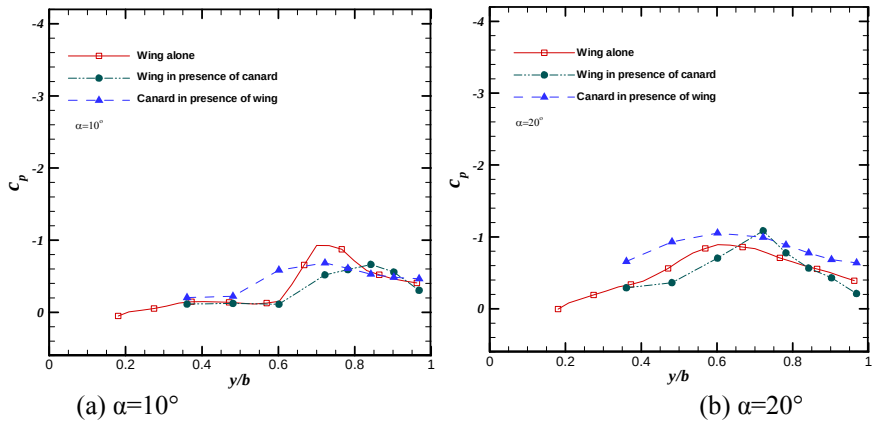

(a) α=10° (b) α=20°

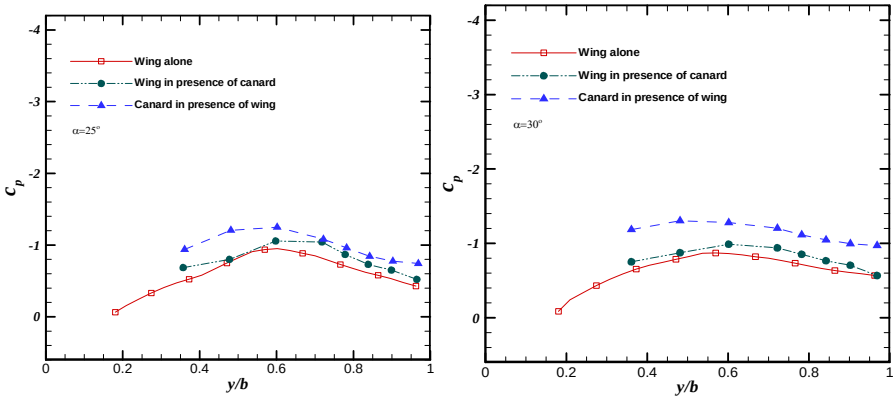

(c) α=25° (d) α=30°

Fig. 13. Spanwise pressure distribution at x/c=0.875

REFERENCES

1. Behrbohm, H. (1965). Basic Low speed aerodynamics of the short-coupled canard configuration of small aspect ratio. *SAAB Aircraft Co. TN-60, Linkoping*, Sweden.
2. Gloss, B. B. & McKinney, L. W. (1973). Canard-wing lift interference related to maneuvering aircraft at subsonic speeds. *NASA TM X-2897*.
3. Gloss, B. B. (1974). The effect of canard leading-edge sweep and dihedral angle on the longitudinal and lateral aerodynamic characteristics of a close-coupled canard-wing configuration. *NASA TN D-7814*.
4. Gloss, B. B. (1074). Effect of canard location and size on canard-wing interference and aerodynamic-center shift related to maneuvering aircraft at transonic speeds. *NASA TN D-7505*.
5. Oelker, H. Chr. & Hummel, D. (1989). Investigations on the vorticity sheets of a close-coupled delta-canard configuration. *ICAS Proceedings*, Vol. 1, 1988, pp. 649-662; see also *Journal of Aircraft*, Vol. 26, No. 7, pp. 657-666.
6. Hummel, D. & Oelker, H. Chr. (1989). Effects of canard position on the aerodynamic characteristics of a close-coupled canard configuration at low speed. *AGARD-CP-465*, pp. 7-1-7-18; see also *Zeitschrift fur Flugwissenschaften und Weltraumforschung*, Vol. 15, No. 2, pp. 74-88.
7. Howard, R. M. & Kersh, J. M. Jr. (1991). Effect of canard deflection on enhanced lift for a close-coupled-canard configuration. *AIAA Paper 91-3222-CP*.
8. Howard. R. M. & O'Leary. J. F. (1994). Flow field study of a close-coupled canard configuration. *Journal of Aircraft*, Vol. 31, No. 4.
9. Zhiyong, L. (1997). A study on flow patterns and aerodynamic characteristics for canard—double delta wing configuration. *AIAA Paper 97-0324*.
10. Hayashibara, S., Myose1, R. Y. & Miller, L. S. (1997). The effect of a 70° swept canard-on the leading edge vortices of a 70° swept delta wing during dynamic pitching. *AIAA Paper 97-0613*.
11. Guy, Y., Morrow, J. A. & McLaughlm, T. E. (1999). The effects of canard shape on the aerodynamic characteristics of a generic missile configuration. *AIAA Paper 99-4256*.
12. Guy, Y., McLaughlm, T. E. & Morrow, J. A. (2000). Effects of canard shape on the center of pressure of a generic missile configuration. *AIAA Paper 2000-0264*.
13. Bergmann. A. & Hummel, D. (2001). Aerodynamic effects of canard position on a wing body configuration in symmetrical flow. *AIAA Paper 2001-0116*.
14. Tu, E. L. (1992). Navier-stokes simulation of a close-coupled canard-wing-body configuration. *Journal of Aircraft*, Vol. 29, No. 5, pp. 830–838.
15. Tu, E. L. (1994). Effect of canard deflection on close-coupled canard-wing-body aerodynamics. *Journal of Aircraft*, Vol. 31, No. 1, pp. 138–145.
16. Ekaterinaris, J. A. (1995). Analysis of flow fields over missile configurations at subsonic speeds. *Journal of Spacecraft and Rockets*, Vol. 32, No. 3, pp. 385– 391.
17. Tuncer, I. H. & Platzer, M. F. (1996). A computational study of a close-coupled delta canard-wing-body configuration. *AIAA Paper 96-2440-CP*.
18. Yoshimoto, M. & Uchiyama, N. (2003). Optimization of canard surface positioning of supersonic business jet for low boom and low drag design. *AIAA Paper 2003-3576*.
19. Joshi, A. & Suryanarayan, S. (2005). Optimal location and size of canards for aeroelastic actuation in aerospace vehicles. AIAA Paper 2005-6330.
20. Rae, H. W., Jr. & Pope, A. (1984). *Low-speed wind tunnel testing*, John Wiley & Sons, Inc.

21. Thomas, G. B., Roy, D. M. & John, H. L. V. (1993). *Mechanical measurements*. Addison-Wesley Publishing Company, 1993.
22. Soltani, M. R., Askari, F., Davari, A. R. & Nayebzade, A. (2010). Effects of canard position on the wing surface pressure. *International Journal of Science and Technology, Scientia Iranica, Transaction B: Mechanical Engineering*, Vol. 17, No. 2, pp. 102-107.
23. Malcolm, G. N. (1981). Impact of high alpha aerodynamics on dynamic stability parameters of aircraft and missiles. *AGARD Lecture Series No. 114*.